



The interplays among meteorology, source, and chemistry in high particulate matter pollution episodes in urban Shanghai, China

Lulu Zeng ^{a,b}, Dan Dan Huang ^{b,*}, Shuhui Zhu ^{b,c}, Fangbing Li ^a, Min Zhou ^b, Liping Qiao ^b, Qian Wang ^b, Qiongqiong Wang ^d, Yingge Ma ^b, Shengrong Lou ^b, Huabin Shi ^{a,e}, Ka In Hoi ^a, Kai Meng Mok ^a, Xinlei Ge ^f, Hongli Wang ^b, Jian Zhen Yu ^{c,d}, Cheng Huang ^b, Yong Jie Li ^{a,*}

^a Department of Civil and Environmental Engineering, Centre for Regional Oceans, Faculty of Science and Technology, University of Macau, Taipa, Macau 999078, China

^b State Environmental Protection Key Laboratory of Formation and Prevention of the Urban Air Pollution Complex, Shanghai Academy of Environmental Sciences, Shanghai 200233, China

^c Division of Environment and Sustainability, Hong Kong University of Science and Technology, Hong Kong, China

^d Department of Chemistry, Hong Kong University of Science and Technology, Hong Kong, China

^e The State Key Laboratory of Internet of Things for Smart City, University of Macau, Taipa, Macau, China

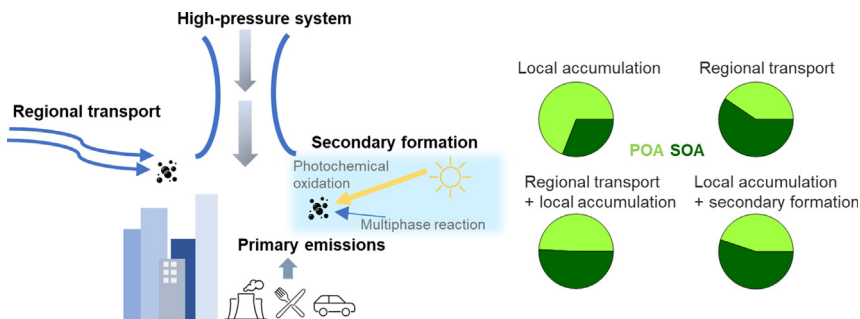
^f Jiangsu Key Laboratory of Atmospheric Environment Monitoring and Pollution Control, Collaborative Innovation Center of Atmospheric Environment and Equipment Technology, School of Environmental Science and Engineering, Nanjing University of Information Science and Technology, Nanjing 210044, China



HIGHLIGHTS

- Meteorology interacts with emission and chemistry to affect OA characteristics.
- SOA formation was mainly affected by photochemical reaction during the campaign.
- In some periods, the production of SOA was promoted by multiphase reaction.
- OA aged in different situations had a similar level of oxygenation.

GRAPHICAL ABSTRACT



ARTICLE INFO

Editor: Pavlos Kassomenos

Keywords:

PM₁
Organic aerosol
Chemical conversion
Weather condition
AMS

ABSTRACT

High particulate matter (PM) pollution episodes still occur occasionally in urban China, despite of improvements in recent years. Investigating the influencing factors of high-PM episodes is beneficial in the formulation of effective control measures. We herein present the effects of weather condition, emission source, and chemical conversion on the occurrence of high-PM episodes in urban Shanghai using multiple online measurements. Three high-PM episodes, i.e., locally-accumulated, regionally-transported, and dust-affected ones, as well as a clean period were selected. Stagnant air with temperature inversion was found in both locally-accumulated and regionally-transported high-PM episodes, but differences in PM evolution were observed. In the more complicated dust-affected episode, the weather condition interacted with the emission/transport sources and chemical conversion, resulting in consecutive stages with different PM characteristics. Specifically, there were (1) stronger local accumulation in the pre-dust period, (2) dust-laden air with aged organic aerosol (OA) upon dust arrival, (3) pollutants being swept into the ocean, and (4) back to the city with aged OA. Our results suggest that (a) local emissions could be rapidly oxidized in some episodes but not all, (b) aged OA from long-range transport (aged in space) had a similar degree of oxygenation compared

* Corresponding authors.

E-mail addresses: huangdd@saes.sh.cn (D.D. Huang), yongjeli@um.edu.mo (Y.J. Li).

to the prolonged local oxidation (aged in time), and (c) OA aged over land and over the ocean were similar in chemical characteristics. The findings help better understand the causes and evolution of high-PM episodes, which are manifested by the interplays among meteorology, source, and chemistry, providing a scientific basis for control measures.

1. Introduction

Particulate matter (PM) pollution in urban areas has received growing attention due to its effects on human health, global climate, and visibility. The toxic substances in PM can enter the human body through respiration, thereby affecting the respiratory (Xing et al., 2016) and cardiovascular (Brook et al., 2010) systems. The abilities of PM to scatter and absorb solar radiation affect the energy balance of the global climatic system (Fiore et al., 2015; Lohmann and Feichter, 2005; Ramanathan et al., 2001) as well as the vitality of ecological system (Wang et al., 2021; Yue et al., 2017). In addition, some particles can act as cloud condensation nuclei (CCN), which affects the albedo of cloud (Twomey, 1977) and the cloud lifetime (Albrecht, 1989), thereby indirectly influencing climate (Forster et al., 2007; Liu et al., 2018). Furthermore, light scattering by PM leads to reduced visibility, which can have impacts on traffic and economic activities (Seinfeld and Pandis, 2016; Watson, 2002).

With rapid economic developments in the last few decades, PM pollution events occur frequently in metropolitan areas in China, e.g., those in North China Plain (NCP), Yangtze River Delta (YRD), and Pearl River Delta (PRD) (Jin et al., 2017; Li et al., 2017). In megacities, anthropogenic emissions and secondary formation are both important PM sources (He et al., 2020; Huang et al., 2019; Lee et al., 2015; Wang et al., 2019b). In recent years, pollution control strategies have been implemented statewide in China, mainly focusing on primary emissions. The measures helped alleviate air pollution levels by substantially reducing primary pollutants. At the same time, secondary pollution, whose formation involves multiple precursors and complex mechanisms, becomes more important, which makes further abatement more challenging. It is thus crucial to investigate the precursor sources and formation mechanisms of secondary pollutants, for instance, secondary organic aerosol (SOA), for deeper abatement of PM pollution.

Numerous studies on PM pollution episodes in urban areas have been conducted in China in recent years (Li et al., 2021b; Sun et al., 2016a; Sun et al., 2014; Yang et al., 2015). In those studies, the causes of high-PM episodes were normally discussed with three different attributes. The first attribute includes primary emission and secondary formation, the latter of which involves chemistry after emissions of gaseous precursors. High-PM pollution events were often accompanied by a synergistic effect of large primary emissions, i.e., from vehicles, coal combustion, biomass burning, cooking, etc., and intense secondary formation via photochemical oxidation and multiphase reactions (An et al., 2019; Huang et al., 2014; Sun et al., 2016b). A good example to demonstrate the importance of secondary formation is that during the COVID-19 lockdown in China with much reduced primary emissions, severe PM pollution episodes were still found in some megacities due to the enhanced secondary formation (Huang et al., 2021b; Zhu et al., 2021b).

The secondary attribute consists of local accumulation and regional transport, which are related to meteorological conditions. The stagnant atmospheric condition is the key factor controlling the accumulation of PM pollutants with low wind speed (WS), high relative humidity (RH), low boundary layer, and anticyclone (Cheng et al., 2018). Regional transport is facilitated by favorable meteorological circulations that bring pollutant-laden air masses from surrounding or even long-distance sources. For instance, Beijing is frequently affected by the pollutants from the surrounding areas in the NCP (Liu et al., 2020; Sun et al., 2016a), as well as dust storms from the Mongolian Plateau (Tian et al., 2018; Yang et al., 2020). Likewise, the megacity Shanghai is often affected by pollution transported from North China and the surrounding industrially developed provinces in the

YRD (Ma et al., 2019; Xu et al., 2015). Shanghai, where we conducted our measurements, is the largest city in the country in terms of both population (>25 million) and economy (GDP in 2019 > 3.8 trillion RMB).

The third attribute includes source strength, chemical conversion, and weather condition, and integrates most of the elements in the first two attributes. The contribution of the source strength to the pollution can be investigated by monitoring and simulation (Liu et al., 2019; Zhang et al., 2016). Activities that enhance the emission source in a short period, e.g., straw burning in harvest seasons, may cause high-PM events in some areas (Li et al., 2008). Chemical processes sometimes worsen the pollution in a number of ways. For example, the decrease of sulfur dioxide increases the ability of ammonia to convert nitric acid to nitrate (Leung et al., 2020), which is a secondary inorganic ion in PM surpassing sulfate in terms of mass contribution in urban China. Weather condition provides favorable conditions for accumulation and/or transport. In particular, high-pressure system (Xu et al., 2011), cold front (Xu et al., 2015), and downdraft outside a tropical cyclone (Wu et al., 2013) are all contributing factors to high-PM events. The third attribute is thus more comprehensive in terms of the causes of high-PM events, as it encompasses most of the key elements that are conducive to a PM episode. While the first two attributes are still widely used in the discussion of the causes of high-PM episodes, the overlapping of these two attributes (primary emission vs. secondary formation, and local emission vs. regional transport) is common. For instance, Tong et al. (2020) reported a high-PM episode in Shanghai caused by the regional transport of biomass burning in a short term, and the episode was also accompanied by secondary formation.

With rapid economic developments in the last few decades, PM pollution events occur frequently in metropolitans. As such, the interplays among weather condition, emission source, and chemical conversion may keep changing the PM pollution level and modifying the PM chemical characteristics. Therefore, in-depth analysis on the causes of PM pollution events requires corroborative evidence from meteorological, statistical, and chemical analyses. The effects of the first and second attributes on high-PM events have been extensively studied in the literature. The interplay among all the three elements in the third attribute has not been thoroughly studied. The objective of this study was to elucidate OA evolution during high-PM episodes, and identify the meteorological influences on accumulation and transport, as well as the chemical processes that lead to elevated SOA formation.

In this study, we deployed a suite of instrument to comprehensively characterize PM chemical compositions, especially the OA components, in real-time at an urban site in Shanghai in the autumn of 2019, which represents a transition from strong photochemistry in summer to intense regional transport in winter. We mainly focus on the organic components in PM, but data of other species are also discussed to reveal the source and chemistry. Aided by meteorological analyses, we ascribed the emission sources and investigated the chemical evolution of PM in three typical episodes, namely locally-accumulated, regionally-transported, and dust-affected ones. Insights on the similarity and difference between different high-PM episodes as related to PM emission sources and formation processes under different meteorological conditions are provided.

2. Experimental section

2.1. Sampling site and instrumentation

The observations were conducted at the Shanghai Academy of Environmental Sciences (SAES, 31.17°N, 121.43°E) from 15 October to 15

November 2019 in the city center of Shanghai. The location of the SAES site is shown in Fig. S1 in the Supplementary Information (SI). The sampling location is surrounded mainly by residential and commercial areas, which contribute to local emissions via activities such as cooking and traffics (Zhu et al., 2021a). At times, regional transport from the neighboring provinces of Jiangsu, Zhejiang, and Anhui, which are among the most developed ones in the country, can also affect the air quality of the site.

The chemical composition of particulate species was characterized by a suite of real-time or semi-continuous instruments. Specifically, the non-refractory components in PM_1 (NR- PM_1), including nitrate (NO_3^-), sulfate (SO_4^{2-}), ammonium (NH_4^+), chloride (Cl^-), and organic aerosol (OA), were measured with the HR-ToF-AMS (ARI, USA). The HR-ToF-AMS was operated with a mass resolution of $(m/\Delta m) \sim 2000$ under V mode at 150 s sampling intervals. The collected AMS data were processed by the standard data analysis software (SQUIRREL 1.60P and PIKA 1.12P) based on Igor Pro (WaveMetrics). In consideration of the conditions of potentially high nitrate content, high RH, and high acidity in the particles, component-dependent collection efficiency (CDCE) was applied to the HR-ToF-AMS data (Middlebrook et al., 2012).

An array of auxiliary measurements was also available at this site, including water-soluble inorganic ions in $\text{PM}_{2.5}$ (SO_4^{2-} , NO_3^- , Cl^- , and NH_4^+), gaseous species (CO, SO_2 , NO, NO_2 , and O_3), organic carbon and elemental carbon (OC/EC), trace elements, molecular tracers, and volatile organic compounds (VOCs) (see Section S1 in the SI for details). The estimation of liquid water content (LWC) concentration contains two parts, the LWC associated with the inorganic species in $\text{PM}_{2.5}$, which was calculated by E-AIM II model (Clegg et al., 1998), and the LWC associated with OA, which was estimated by the equation from Petters and Kreidenweis (2007). The details are given in Section S2 and Fig. S2 in the SI.

2.2. Positive matrix factorization (PMF) analysis

The sources of organic aerosol (OA) were resolved by using the PMF2 algorithm (Paatero et al., 2002), using the PMF Evaluation Toolkit version 3.04A (Ulbrich et al., 2009) based on Igor Pro, which has been described extensively in the literature (Ulbrich et al., 2009; Zhang et al., 2011). Thus, only a brief description is provided here and in Section S3 in the SI. The OA mass spectra between m/z 10 and 150 were utilized for PMF analysis. PMF analysis has been performed both on AMS dataset alone (AMS-PMF) as well as on the combined data matrix of AMS and a thermal desorption aerosol gas chromatography-mass spectrometer (TAG) measurements (integrated-PMF), the latter of which was conducted to interpret the OA factors with the molecular tracer information and also to support the AMS-PMF analysis. The mass spectral profiles, time series, and diurnal patterns of OA components for a number of solutions were carefully examined and a seven-factor solution with fPeak = 0 was adopted. The key diagnostics of the PMF analysis are presented in Section S4 and Fig. S3 in the SI and had also been detailed in our previous study (Huang et al., 2021a). The OA factors in the selected solution include four primary factors, namely, hydrocarbon-like organic aerosol factors (HOA1 and HOA2) and cooking organic aerosol (COA) factors (primary COA, PCOA, and oxidized COA, OCOA), as well as three secondary factors, namely, less-oxidized oxygenated organic aerosol (LO-OOA1 and LO-OOA2), and more-oxidized oxygenated organic aerosol (MO-OOA).

2.3. Meteorological data

Meteorological parameters such as WS, wind direction (WD), temperature, and RH were obtained from the weather station at Shanghai Hongqiao International Airport, which is <10 km from the sampling site. Other meteorological data, including mean sea level pressure, horizontal and vertical wind field data ($0.25^\circ \times 0.25^\circ$ resolution), were from the European Centre for Medium-Range Weather Forecasts (<https://cds.climate.copernicus.eu/>). Vertical profiles of temperature were obtained from the University of

Wyoming, recorded twice every day at 08:00 and 20:00 (<http://weather.uwyo.edu/wyoming/>).

The 72-hour air mass back trajectories were calculated every hour at 500 m above the ground level using the Hybrid-Single Particle Lagrangian Integrated Trajectory (HYSPART) model (<https://www.arl.noaa.gov/>). After calculating multiple back trajectories in each period, the trajectories close to each other were merged into clusters as mean trajectories. The optimum number of clusters was determined by the total spatial variance (TSV) (Stein et al., 2015).

3. Results and discussion

3.1. Overview of the campaign

We first begin with an overview of the measurement data (Figs. 1 and S4). The average concentration of the NR- PM_1 ($\text{SO}_4^{2-} + \text{NO}_3^- + \text{NH}_4^+ + \text{Cl}^- + \text{OA}$) during the campaign was $16.5 \pm 9.5 \mu\text{g}/\text{m}^3$, with more than a half contributed by OA (53.3%). During our campaign, Shanghai was dominated by northerly winds (Fig. S5) with the average WS, temperature and RH of 3.2 m/s, 18.1 °C and 63.1 %, respectively (Table S1). The diurnal variations of solar radiation (SR), RH, temperature, as well as LWC and O_x ($= \text{O}_3 + \text{NO}_2$) mixing ratio are shown in Fig. 2a and b. There are typical opposite trends for temperature and RH driven by their intrinsic anti-correlated relationship, as well as for O_x and LWC driven by photochemistry during the day and efficient condensation of water vapor during the night. Also shown in Figs. 2 and S6 are the diurnal variations of different NR- PM_1 species and OA factors. The description of the diurnal variations of inorganic species can be found in Section S5 in the SI.

We mainly focus on the sources and formation routes of the OA components in this study. The diurnal variation of OA (Fig. 2c) presents three peaks during 06:00–08:00, 12:00–13:00, and 18:00–20:00, which is similar to those reported earlier in megacities in China, such as Shanghai (Zhu et al., 2021c), Beijing (Hu et al., 2017), Nanjing (Zhang et al., 2015), and Shenzhen (Cao et al., 2018). The diurnal patterns of OA factors resolved by PMF analysis are shown in Fig. 2d, and their characteristics are discussed in paragraphs that follow or provided in Section S6 in the SI.

The HOA factors (HOA1 and HOA2) peaked in the morning and evening rush hours (Fig. 2d). The HOA factors were well correlated with NO_x and BC as well as molecular tracers such as alkanes and polycyclic aromatic hydrocarbons (PAHs), indicating their origination from vehicular emissions (Schauer et al., 2002; Wang et al., 2019a). Furthermore, HOA2 shows strong associations with aromatic SOA tracers, such as 1,2,4-benzenetricarboxylic acid, 1,3,5-benzenetricarboxylic acid (BTCAs) and 2,3-dihydroxy-4-oxopentanoic acid (DHOPA), suggesting that HOA2 was likely derived from the oxidation of HOA1 and/or co-emitted gaseous vehicular pollutants. Besides HOA factors, primary OA (POA) factors associated with catering activities (PCOA and OCOA) were also identified. The OCOA factor is believed to form from the in situ oxidation and rapid transformation of freshly emitted PCOA. Details on the identification of COA factors can be found in our companion study (Huang et al., 2021a). In this study, both HOA2 and OCOA are considered as POA factors since they are tightly related to the directly emitted OA factors (HOA1 and PCOA, respectively).

Depending on the degree of oxygenation, oxygenated organic aerosol (OOA) was further separated into LO-OOA and MO-OOA factors. The sum of OOA factors (LO-OOA + MO-OOA, 48.8 %) shows a similar contribution as the sum of POA factors (51.2 %) during the campaign. The LO-OOA was further separated into LO-OOA1 and LO-OOA2. From the diurnal pattern (Fig. 2d), one can see that LO-OOA1 was likely formed during the day and accumulated until night. There were strong correlations ($R^2 = 0.70\text{--}0.81$) between the LO-OOA1 and SOA tracers measured with the TAG (Fig. S9), including the α -pinene-derived SOA tracer, dicarboxylic acids (DCAs), and DHOPA. These good correlations indicate that LO-OOA1 probably consists of freshly formed products from the oxidation of biogenic and anthropogenic VOCs (Ervens, 2004; Kautzman et al., 2010; Zhu et al., 2021a). On the contrary, there is no strong correlation between

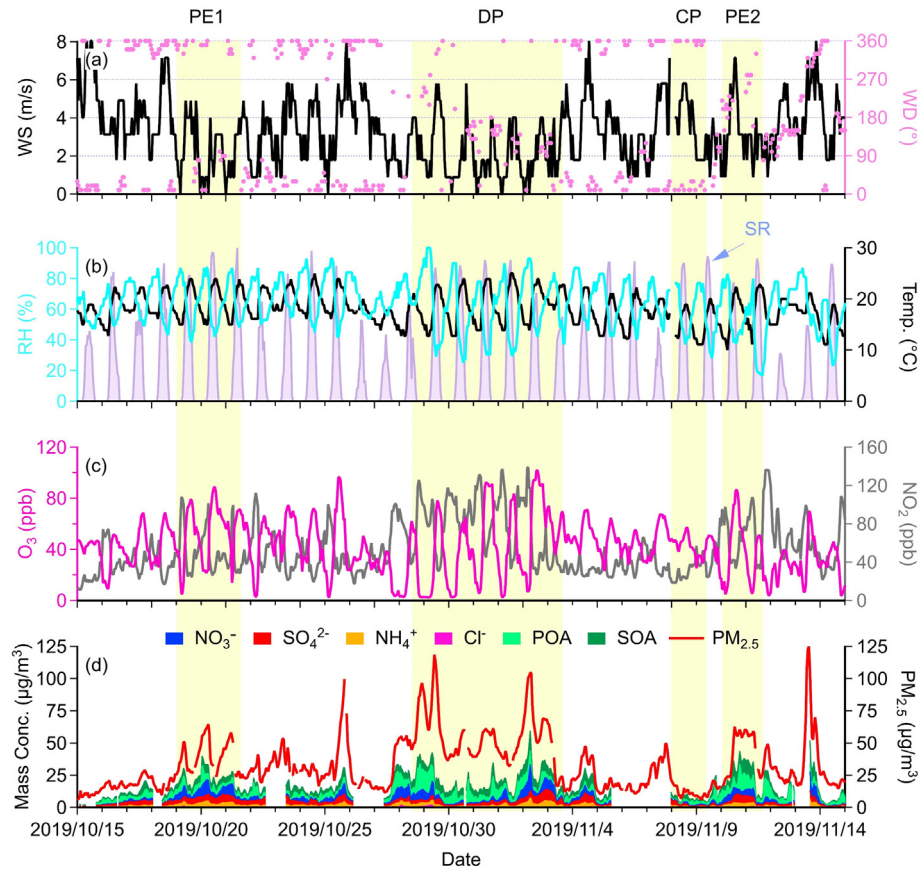


Fig. 1. Time series of (a) wind speed (WS) and wind direction (WD), (b) relative humidity (RH), temperature, and solar radiation (SR), (c) concentrations of O₃ and NO₂, and (d) concentrations of PM_{2.5} and NR-PM₁ components.

LO-OOA2 and TAG tracers (Fig. S9); in addition, LO-OOA2 contributes only about 4.0 % to 9.3 % to total OA in all periods. We believe that the LO-OOA2 might be a mixed OA factor. There was an obvious increase of MO-

OOA in the daytime starting from 06:00 till 14:00, during which it reached its maxima (Fig. 2d). Previous studies (Hu et al., 2022; Li et al., 2021a) have suggested that high WS in daytime might facilitate regional transport of

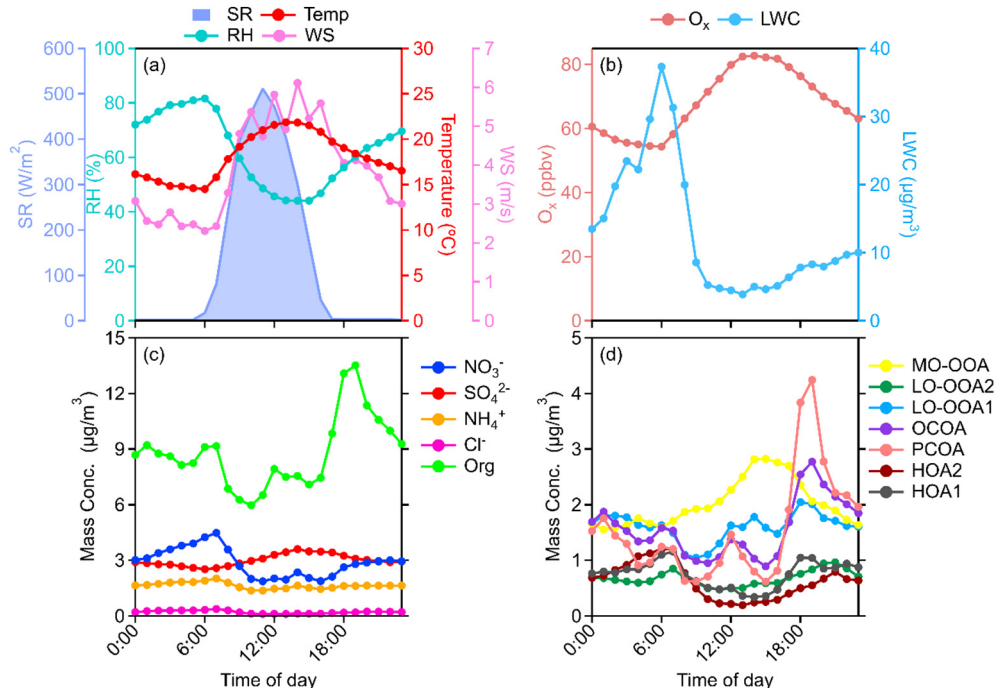


Fig. 2. The diurnal variations of (a) meteorological parameters, (b) LWC and O_x (= O₃ + NO₂), (c) NR-PM₁ components, and (d) OA factors.

aged OA to urban sites. The WS in our study increased from 09:00 to 16:00 (Fig. 2a), alongside with high SR during the day. Therefore, we believe that the high concentrations of MO-OOA during the day might be due to the combined effect of daytime regional transport of aged OA and local photochemical oxidation.

Odd oxygen ($O_x = NO_2 + O_3$) has been widely used to indicate the photochemical activity (Huang et al., 2021c; Wood et al., 2010). Fig. S10 shows the correlations between the summed concentrations of OOA factors (LO-OOA1 + LO-OOA2 + MO-OOA, as a surrogate of SOA) vs. O_x and LWC for the whole campaign, as well as those for daytime and nighttime data. The daytime peaks of OOA factors (10:00–18:00, Fig. 2d) and their stronger correlations with O_x (Fig. S10b, $R^2 = 0.57$) imply that SOA formation in our study is affected by oxidative capacity and is largely contributed by photochemical reactions. Meanwhile, SOA also shows a fairly strong correlation with LWC during daytime (Fig. S10e, $R^2 = 0.54$), although LWC during the day is relatively low compared to that at night. Yet, a careful

examination on Fig. S10e shows that high SOA concentrations correspond to high concentrations of both LWC and O_x . Hence, we also examined the correlation between SOA and LWC during nighttime, which is weaker than that during the daytime (Fig. S10f). Therefore, we conclude that photochemical processes dominated SOA formation at our site in general. Despite this, we cannot completely exclude the contributions from multiphase processes to SOA formation (or secondary aerosol formation in general), especially during certain episodic events, which will be discussed later. For example, good correlations were found between NO_3^- and LWC (Fig. S11), indicating nighttime formation of nitrate via multiphase reactions.

3.2. Episodic events

During the campaign, 41.3 % of air mass trajectories were from northern China such as the NCP, and 45.6 % were from even further northwest

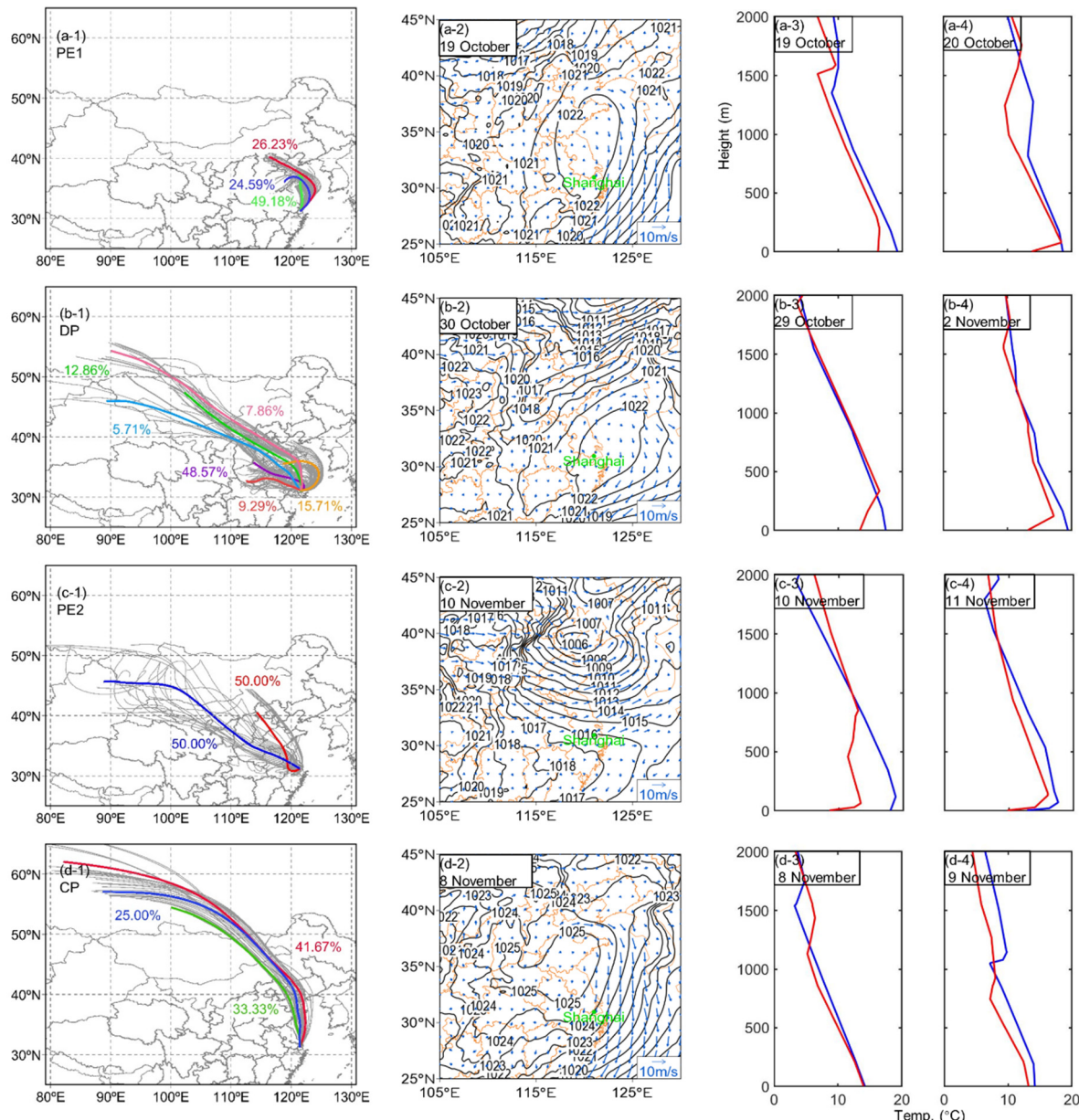


Fig. 3. Summary of weather conditions during the four selected periods (PE1, DP, PE2, and CP). (a-1) to (d-1): 72-hour back trajectory clusters at a height of 500 m. The weather fields show the average surface wind pattern (arrows) and sea level pressure (line) on (a-2) 19 October, (b-2) 30 October, (c-2) 10 November, and (d-2) 8 November. (a-3), (a-4) to (d-3), (d-4) are vertical temperature profiles at (red) 08:00 and (blue) 20:00.

including Mongolia and beyond (Fig. S12). There was a dust storm event from 29 October to 3 November that brought in dust particles and resulted in high PM₁₀ concentrations (maximum hourly concentration of 466.0 $\mu\text{g}/\text{m}^3$) in Shanghai (Fig. S13a). Given the differences in meteorological patterns (Fig. 3) as well as the air mass origins during the campaign, three episodic and one clean periods (Table S2), namely pollution episode 1 (PE1, 19–21 October), pollution episode 2 (PE2, 10–11 November), dust period (DP, 28 October to 3 November), and clean period (CP, 8–9 November), were selected for further analysis. The average mass concentrations of PM₁ during the three episodic ranged from 22.2 to 27.2 $\mu\text{g}/\text{m}^3$, which were 3 to 4 times higher than that observed during the clean period CP. Detailed information on the meteorological parameters for different periods is summarized in Table S1.

The meteorological conditions of the four selected periods were quite distinct. PE1 was controlled by a high-pressure anticyclone, while PE2 was influenced by a low-pressure system located in northeastern China and air flow from the north transported pollutants to Shanghai. During DP, the dust storm from the Mongolian Plateau arrived in Shanghai. In CP, Shanghai was influenced by clean air flows from the upper level and there was no significant pollution in the nearby region of Shanghai (Fig. S14). In addition, among the four selected periods, CP was the only

period without significant inversion layer in both morning and evening (Fig. 3). This fairly good meteorological condition for air pollution dispersion resulted in low PM concentrations in CP, with average concentrations of PM_{2.5} and NR-PM₁ of 11.2 and 6.6 $\mu\text{g}/\text{m}^3$, respectively, which were the lowest among the four selected periods.

3.2.1. The locally-accumulated episode (PE1)

The high-pressure anticyclone in PE1 (Figs. 4e, f, and S15) resulted in low WS ($2.3 \pm 1.3 \text{ m/s}$) and a stable atmospheric condition, and strong temperature inversion also occurred (Fig. 3a-4). The height of the inversion layer was below 200 m, and the temperature difference between the top of the inversion layer and the surface was 6 °C. Overall, this weather condition favors the accumulation of pollutants. As a result, a significant increase in EC and NO_x concentration upon accumulation was observed in PE1 (Fig. 4a), which is an indication of strong primary emissions from combustion processes. For instance, POA factors such as HOA1 and HOA2 showed average growth rates of 0.30 and 0.33 $\mu\text{g}/\text{m}^3$ per hour in the early morning on 19 October.

Local accumulation of primary pollutants, however, was not the only reason that led to high pollution levels in PE1. Due to the stagnant condition, the air mass with primary PM and gaseous precursors stayed in the

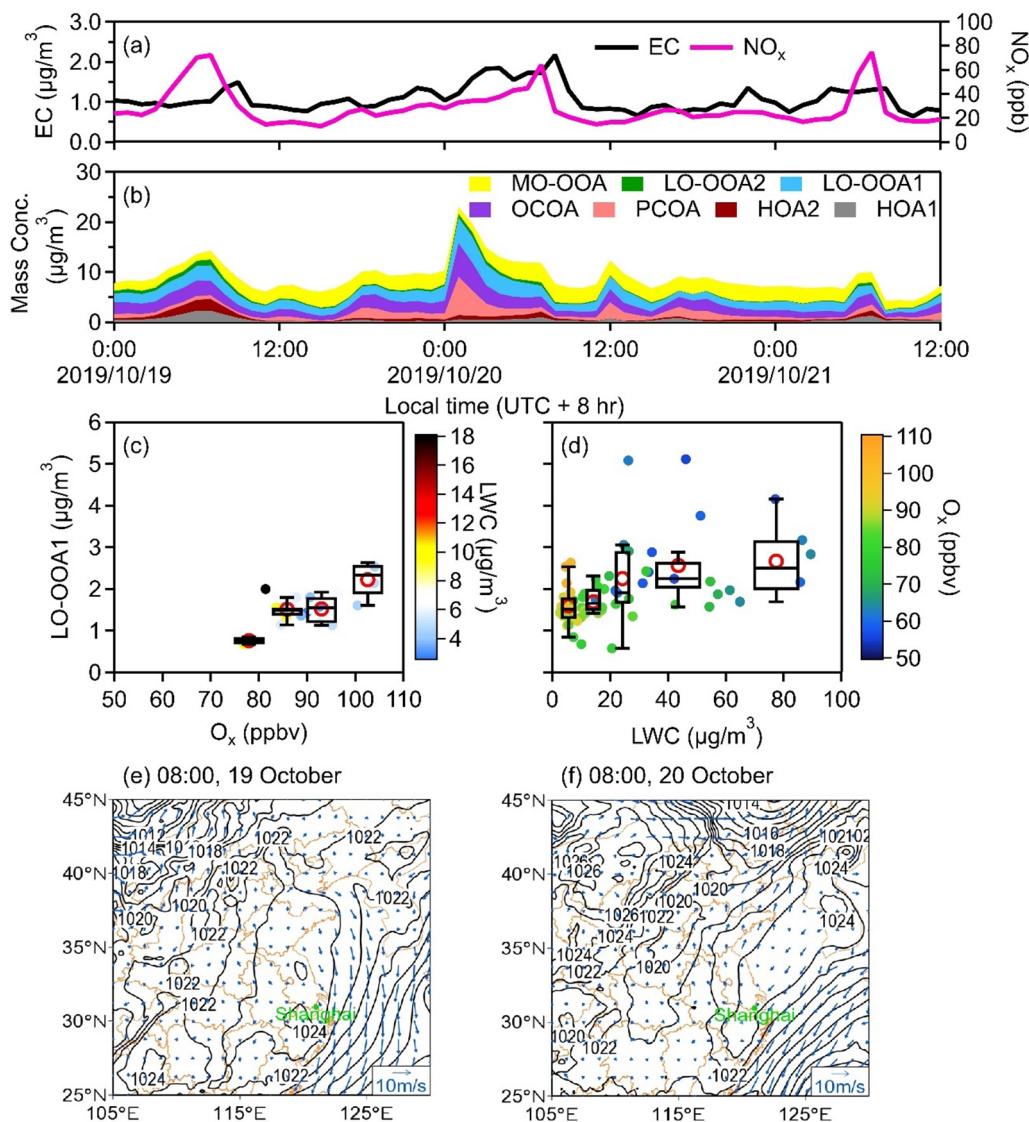


Fig. 4. Time series of (a) EC and NO_x and (b) OA mass concentration. The scatter plots show (c) LO-OOA1 concentration vs. O_x during daytime and (d) LO-OOA1 concentration vs. LWC during daytime and night in PE1. Note that as few data points have LWCs over 30 $\mu\text{g}/\text{m}^3$, the width of the first three bins is 10 $\mu\text{g}/\text{m}^3$, and the width of the last two bins is 30 $\mu\text{g}/\text{m}^3$. The surface weather maps during PE1 at (e) 08:00 on 19 October and (f) 08:00 on 20 October.

city for an extended period of time. Efficient local production of less oxygenated (fresh) SOA was also observed, resulting in the highest fraction of LO-OOA1 in OA (22.1 %) in PE1 among the four selected periods (Fig. S16a). During PE1, the strong solar radiation (701.5 W/m², Fig. 1b), high J(O¹D) value (maximum 2.13×10^{-5} s⁻¹, Fig. S4c), and high O₃ concentration (maximum 89.2 ppb, Fig. 1c) were favorable for local secondary formation (Zhong et al., 2018). Photochemical reactions contributed significantly to the local SOA production as indicated by the good correlation between LO-OOA1 and O_x ($R^2 = 0.70$, Figs. 4c and S17), which is similar to the observation in Beijing (Xu et al., 2017). On the other hand, we also observed a higher ratio of OCOA to PCOA (1.8) in PE1 than those in the other three periods (0.7 in DP, 0.7 in PE2, and 1.5 in CP), which is an indication of efficient local conversion from freshly emitted OA to more oxygenated ones.

It is interesting to note that high LO-OOA1 concentration (2.2 $\mu\text{g}/\text{m}^3$, the average concentration in the last bin in Fig. 4c) occurred at high O_x concentration (O_x > 100 ppbv) but low LWC concentration (LWC < 6 $\mu\text{g}/\text{m}^3$) during daytime (Fig. 4c). During the night, the concentration of LO-OOA1 was even higher (2.7 $\mu\text{g}/\text{m}^3$, the average concentration in the last bin in Fig. 4d) when LWC was high (LWC > 80 $\mu\text{g}/\text{m}^3$), although O_x concentration was lower (O_x between 57.1 ppbv and 65.9 ppbv, Fig. 4d). This high LO-OOA1 concentration associated with high LWC and low O_x is an indication of the contribution from multiphase reactions. In addition, a strong correlation between the LWC and the NO₃⁻ concentration was also observed during PE1 ($R^2 = 0.79$, Fig. S18), which was attributed to multiphase chemistry (Zhu et al., 2021c). Therefore, although SOA formation during

the whole campaign was dominated by photochemical reactions, multiphase chemistry might play an important role in PE1 in the formation of SOA and nitrate. In a quick summary, our analysis suggests that PE1 was a locally accumulated PM pollution episode accompanied by efficient local secondary formation.

3.2.2. The regionally-transported episode (PE2)

PE2 experienced a change in the weather system. In the early stage of PE2, a cyclone system located in northeast China facilitated the transport of pollutants from the north (Fig. 5d). Before the air mass arrived in Shanghai, a severe pollution event occurred at the NCP region upwind of YRD during 8–9 November (Fig. 5c). Hence, on the first day of PE2 (10 November), high levels of air pollutants were transported from the NCP to Shanghai, resulting in high PM levels. In a later stage of PE2, however, a strong temperature inversion occurred on 11 November (Fig. 3c-4). The inversion had temperature differences between the top of the inversion layer and the surface of 6.2 and 5.2 °C in the morning and the evening, respectively, preventing efficient dispersion of air pollutants. Among the four periods, PE2 had the highest mass concentration of MO-OOA (3.3 ± 1.9 $\mu\text{g}/\text{m}^3$), a surrogate of aged SOA, indicating the influence of regional transport. Fig. S19 shows a wind rose plot with OA concentrations, from which high concentrations of MO-OOA and LO-OOA mainly from the northwest region are observed.

Fig. 5 further shows in detail the variations of each OA component in PE2, in which the first stage corresponded to the regional transport while

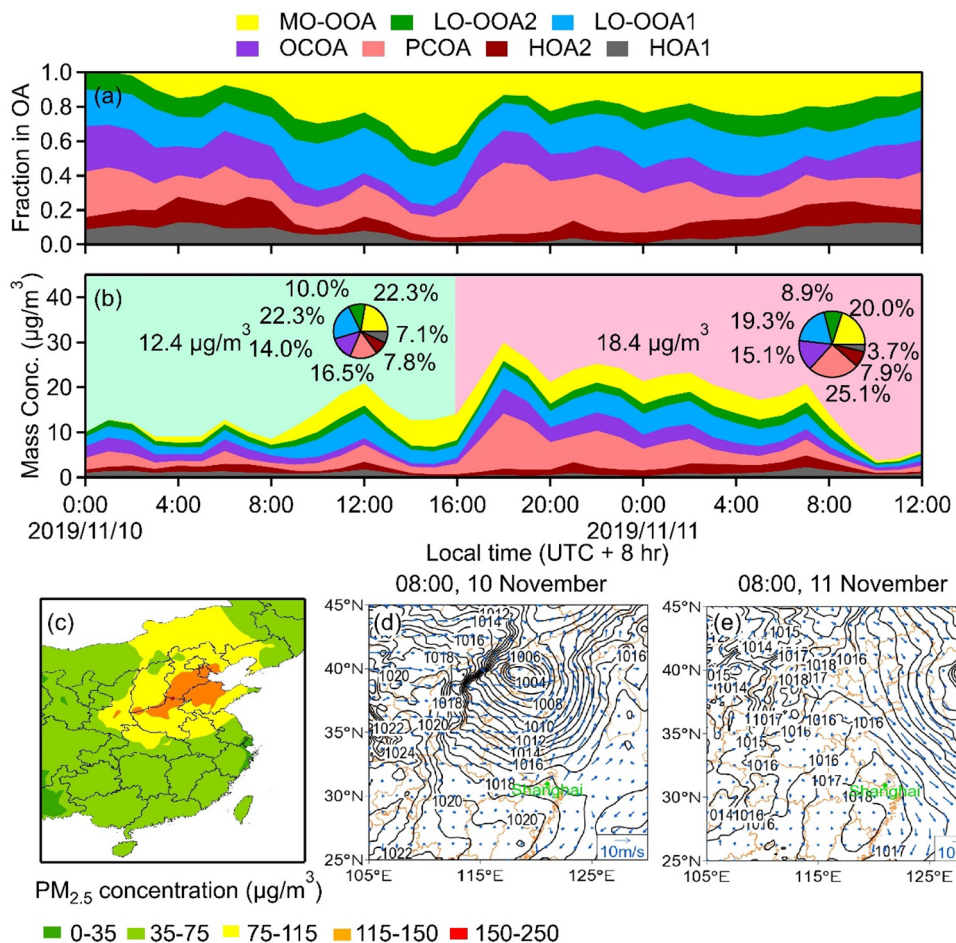


Fig. 5. Time series of (a) fractional contributions and (b) concentrations of OA compositions in PE2. The areas of the pies are proportional to the mass concentrations. Background colors of green and pink respectively denote first and second stages. The pie charts show the contributions of OA factors for two periods, respectively. (c) spatial distribution of PM_{2.5} concentrations in some regions of China on 9 November 2019. The PM_{2.5} data were obtained from the state-controlled air sampling sites in China. The surface weather maps during PE2 at (d) 08:00 on 10 November and (e) 08:00 on 11 November.

the second stage was mainly influenced by local accumulation. The first stage was influenced by the low-pressure system located in the north and the high WS (3.6 ± 2.1 m/s, maximum 5.8 m/s) in Shanghai, and the pollution was mainly from regional transport. In the second stage, Shanghai was mainly controlled by a high-pressure system, the stagnant condition, and decreased WS (2.7 ± 0.8 m/s), and the PM pollution was mainly affected by local accumulation. The time series of OA components shows that the first stage of PE2 (00:00–16:00 on 10 November) is dominated by SOA (54.6 %), and the second stage of PE2 (16:00 on 10 November to 12:00 on 11 November) is dominated by POA (51.8 %). The concentration and fraction of MO-OOA increased in the morning on 10 November, up to $3.0 \mu\text{g}/\text{m}^3$ and 47.8 % in total OA, upon the arrival of the aged air mass from the northwest. From the night of the 10th to the next morning, the low-pressure system located in the Northeast Plain moved eastward (Fig. 5d). Shanghai was then controlled by a high-pressure system (Fig. 5e) with low WS (Figs. 1 and S20). With the inversion layer during the nighttime (Fig. 3c-4), the transported and aged air mass with high PM pollution lingered around Shanghai, and most OA components maintained at high concentrations ($18.4 \pm 7.6 \mu\text{g}/\text{m}^3$) before the next morning (Fig. 5b). At the same time, the concentrations and fractions of POA factors (e.g., PCOA and OCOA) also increased substantially and stayed high till the next morning. The concentration of SOA increased from $6.8 \pm 3.4 \mu\text{g}/\text{m}^3$ in the first stage to $8.9 \pm 3.5 \mu\text{g}/\text{m}^3$ in the second stage, with a growth of 33.0 %. POA concentration increased from $5.6 \pm 1.9 \mu\text{g}/\text{m}^3$ to $9.5 \pm 4.6 \mu\text{g}/\text{m}^3$, with a 69.3 % increase. The increase of POA in the second stage is much larger than that of SOA, indicating that local primary emissions also played an important role in the second stage of PE2. The analysis on PE2 thus suggests that stagnant meteorological conditions after regional transport from nearby regions can significantly deteriorate PM pollution in Shanghai. In short, although PE2 was generally speaking a regionally-transported high-PM event, it was also affected by local accumulation at a later stage of the episode.

3.2.3. The dust period (DP)

The dust period DP was further classified into four stages (Table S2): (1) accumulation of local pollutants before the dust arrival (DP1), (2) the arrival of the dust storm (DP2), (3) the post-dust period when pollutants were gradually pushed out to the East China Sea (ECS) and followed by local pollutant accumulation (DP3), and (4) a period with the backflow of dust from the ECS (DP4). The overall NR-PM₁ composition and OA composition of DP (Fig. S16a) were similar to those in PE2. However, the portion of trace elements in PM_{2.5} in PE2 (16.0 %, Fig. S21) was significantly lower than that in DP (27.3 %), due to the dust origin of the latter.

Before the dust arrival, Shanghai was controlled by a weak convergence system, which was unfavorable for pollutants dispersion, thus the concentration of PM_{2.5} reached $96.6 \mu\text{g}/\text{m}^3$ in DP1 (Fig. 1d). DP1 was a typical local accumulation process, in which POA had the highest fraction in total OA (69 %) among all periods and sub-periods. In this sub-period, the emission and accumulation of PCOA, HOA1, and HOA2 under stagnant meteorological conditions elevated the OA concentration level substantially (Fig. 6a and b). This typical local accumulation process is also supported by the highest average mass concentration of EC ($2.3 \pm 0.6 \mu\text{g}/\text{m}^3$) in DP1 among the four sub-periods in DP.

During DP2, the dust that originated from the northwest of China arrived in Shanghai (Fig. S13a) when the city was under the control of the downdraft at 09:00 on 29 October (Fig. 6c-3). At that time, the high-altitude dust settled to the ground with the rise of the boundary layer. The contribution of trace elements, which were mainly from the soil or dust particles in PM_{2.5}, increased greatly in DP2 (43.2 %) compared to that in DP1 (10.3 %) and remained significant in DP3 (36.1 %) and DP4 (23.4 %) (Fig. S21). The dust-laden air mass brought large amounts of aged pollutants. For instance, the percentage of MO-OOA in total OA increased from 5.4 % in DP1 to 33.1 % in DP2 (Fig. 6a), giving DP2 the characteristics of regional transport similar to the first stage PE2, especially for OA components.

During DP3, the dust was swept out to the ECS, and the concentrations of PM_{2.5} ($46.9 \pm 8.6 \mu\text{g}/\text{m}^3$) and PM₁₀ ($183.6 \pm 60.9 \mu\text{g}/\text{m}^3$) significantly

decreased. The percentage of MO-OOA in total OA in DP3 (22.1 %) decreased significantly compared to that in DP2 (33.1 %). This change in MO-OOA percentage is similar to that for the two stages in PE2, in which MO-OOA decreased slightly from 22.3 % in the first stage to 20.0 % in the second stage. The high percentage of MO-OOA in the first stage of PE2 and that in DP2 point to a common source of OA with regional transport, but the different extents of decreases of MO-OOA fractions afterwards (i.e., the second stage of PE2 and DP3) suggest some difference in the contribution from local accumulation. In the second stage of PE2, transported OA stayed in Shanghai and the MO-OOA fraction decreased only slightly; in DP3, on the contrary, most of the dust-laden air with aged OA (i.e., MO-OOA) was swept out to the sea, leading to a significant decrease in MO-OOA. Evidently, the percentage of POA gradually increased from 40.6 % in DP2 to 53 % in DP3 (Fig. 6a), indicating that local emission became the main sources of OA during DP3.

During DP4, the air mass flew back from the sea (Fig. S13b). As shown in Fig. 6c-4, an updraft was observed over the sea, while the land was controlled by a downdraft. The air mass with dust and pollutant over the sea was lifted by the updraft and transported inland, then the pollutant sank and gathered inland under the influence of the downdraft. This last stage of the dust event (DP4) was characterized by high O₃ ($58.3 \pm 28.6 \text{ ppb}$) and nitrate concentrations ($5.6 \pm 4.4 \mu\text{g}/\text{m}^3$). Similar enhanced formation of O₃ over the South China Sea due to the land-originated air pollutants was also reported previously (Wang et al., 2018a; Wang et al., 2018b). For nitrate, Wu et al. (2020) suggested that NO₃⁻ was formed by the hydrolysis of N₂O₅ on the surface of saline mineral particles (e.g., CaSO₄ and Na₂SO₄), which might be responsible for the high concentration of NO₃⁻ (reaching $20.5 \mu\text{g}/\text{m}^3$, Fig. 1d).

In addition to O₃ and nitrate, SOA might also be formed over the sea and then transported back to the city in DP4. With little emission over the sea, the air mass moved out into the ECS during DP3 and back to Shanghai during DP4 providing a good opportunity to study the SOA formation from anthropogenic precursors, similar to that in a smog chamber. As shown in Fig. 6b, the MO-OOA concentration in DP4 ($3.4 \pm 1.6 \mu\text{g}/\text{m}^3$) indeed increased, suggesting SOA formation over the sea. We estimate SOA formation from aromatic VOCs by a VOC consumption method (Ait-Helal et al., 2014) and a maximum potential method, with details shown in Section S7 in the SI. The SOA estimated by the VOC consumption method was $0.26 \mu\text{g}/\text{m}^3$, and the maximum SOA potential from aromatic VOCs was $0.63 \mu\text{g}/\text{m}^3$ (Fig. 6d). The difference of the measured SOA mass concentration between DP4 and DP3 was $1.29 \mu\text{g}/\text{m}^3$, which can be assumed as the amount of SOA formed over the sea. These estimations indicate that there is still a large discrepancy between the SOA measured and the SOA estimated from known VOC precursors. From the calculation, about 20 % of SOA calculated by the VOC consumption method can be attributed to the measured aromatic VOCs. The contribution of aromatic VOCs estimated by the maximum SOA potential could reach as high as 50 % of the SOA. This comparison suggests that aromatic VOCs contribute to a substantial amount of SOA formation, but other precursors (e.g., aliphatic VOCs) cannot be neglected.

3.3. OA evolution in episodic events

The dynamics of elemental ratios (O:C and H:C) in different periods provide further insights into the evolution of OA in the high-PM episodes and the clean period. Fig. 7 shows the van Krevelen (VK) diagrams during the four selected periods (PE1, DP, PE2, and CP) on the left panel and the four sub-periods in DP (DP1 to DP4) on the right one. In the VK diagram, the data points are clustered in different parts due to different chemical processes (Heald et al., 2010; Li et al., 2015; Ng et al., 2010).

PE1, PE2, DP1, and DP3 were all influenced by local accumulation, albeit at different stages or to different extents. Therefore, the chemical characteristics of OA in these high-PM periods also show some differences because of different influencing factors. The slope in PE1 (-0.74) is significantly shallower than that of DP1 (-0.95), which might be due to the higher contribution of LO-OOA1 (22.1 %) locally formed during PE1 that

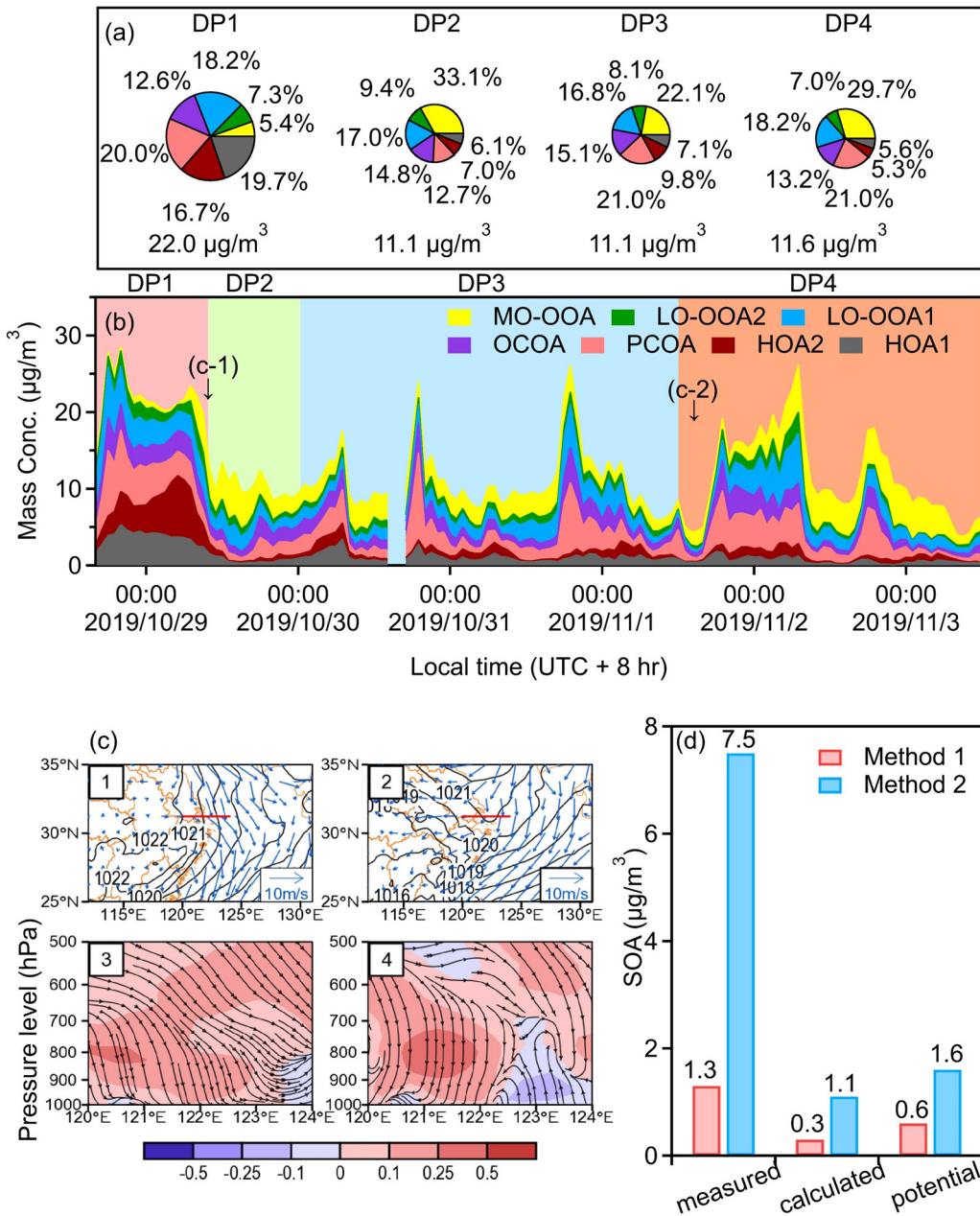


Fig. 6. (a) Mass fractions of OA factors among total OA during DP1 to DP4. The areas of the pies are proportional to the mass concentrations. (b) Time series of OA composition in DP. (c) The horizontal wind field and the vertical cross section at 09:00 on 29 October and at 15:00 on 1 November. Vertical cross section taken over a latitude of 31.23°N (red lines in c-1 and c-2), and the purple color and light red color present downward and upward winds, respectively. (d) The measured consumption of SOA compared to the calculated results, with details provided in main text and SI (Section S7).

resulted in more oxygenated (a higher O:C ratio of 0.44 ± 0.07) OA than that in DP1. During DP1, the local accumulation of HOA1 and HOA2 resulted in the lowest O:C ratio (0.24 ± 0.04) and the highest H:C ratio (1.80 ± 0.04) among the four sub-periods in DP (Fig. 7b). Thus, DP1 is considered as a more “pure” locally-accumulated pollution event. PE2 was affected by both regional transport and local accumulation, thus the slope of PE2 (-0.69) is between those for the more “pure” regionally-transported event (DP2, -0.62) and the more “pure” locally-accumulated event (DP1, -0.95). In DP3, most of the dust-laden OA was swept out to the sea. Therefore, DP3 was less influenced by transported pollutants, which led to a steeper slope (-0.82) for DP3 compared to PE2 (-0.69). The slope of PE2 (-0.69) is closer to that of DP2 (-0.62), while the slope of DP3 (-0.82) is closer to that of DP1 (-0.95). This result also

indicates that PE2 was more influenced by regional transport and DP3 was mainly affected by local accumulation.

The similar slopes of DP2 and CP (-0.62 and -0.61 , respectively) are probably because the pollutants from long-range transport in DP2 (aged in space) had a similar level of oxidation compared to the prolonged local oxidation in CP (aged in time) with excess oxidants compared to precursors. During DP3, the air masses were blown out into the sea, and the source changed to local emissions again, resulting in more similar slopes between DP3 (-0.82) and PE1 (-0.74). When pollutants were oxidized over the sea and transported back to Shanghai in DP4, the higher O:C (0.44 ± 0.10) and lower H:C (1.63 ± 0.07) ratios resulted in a similarly shallow slope in DP4 (-0.68) and PE2 (-0.69). We might consider that air masses arriving at Shanghai during PE2 and DP4 were those aged over the land and

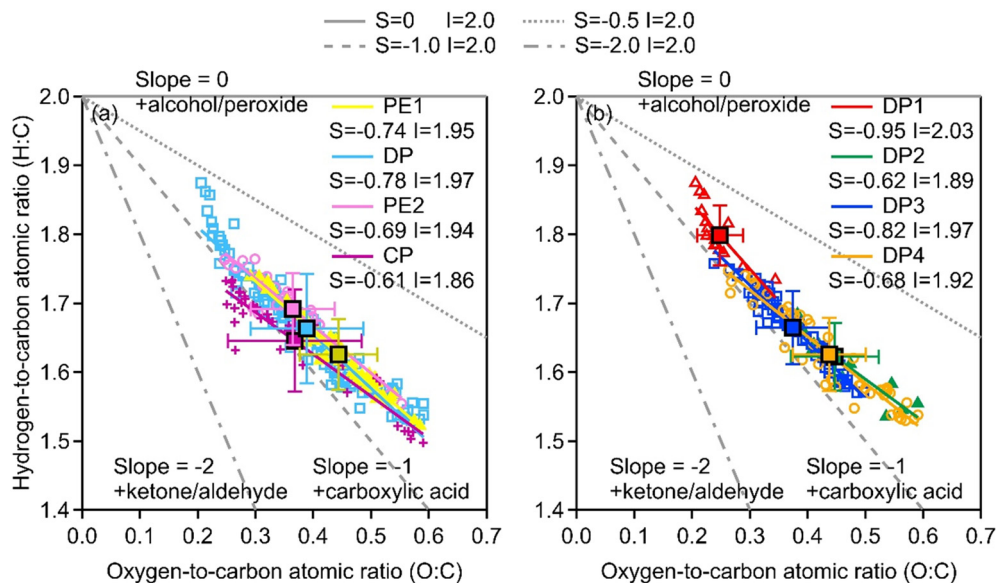


Fig. 7. The van Krevelen diagrams during (a) PE1, DP, PE2, and CP, and (b) DP1 to DP4. The makers denote all data, and the squares with error bars (standard deviations) are the mean values of specific periods. The notation of “S” denotes slope, and “I” denotes intercept.

the sea, respectively. The similar slopes (Fig. 7) in PE2 and DP4 thus suggest that aging in regional transport inland (PE2) and in the marine boundary layer (DP4) might lead to little difference in OA evolution processes, at least for this study.

4. Conclusions

We used a suite of online instruments to investigate the sources and chemical evolution of PM in different pollution episodes in urban Shanghai in autumn 2019. The average concentration of NR-PM₁ was 16.5 µg/m³, in which OA (53.3 %) had the highest contribution. Seven OA factors were resolved by PMF analysis, with the highest contribution of MO-OOA (22.9 %), which indicates that OA was more influenced by regional transport throughout the campaign.

Many studies investigated the evolution and the main factors of high-pollution events (Huang et al., 2012; Lee et al., 2013; Sun et al., 2016a; Sun et al., 2014; Zhang et al., 2018). In this study, three typical high-PM pollution events and one clean period were selected for detailed analysis, with the dust event (DP) further separated into four sub-periods. The evolution of the chemical composition for each pollution period was analyzed regarding weather condition, source strength, and chemical conversion. In our study, the influences from weather condition include stagnant meteorological conditions under the control of high-pressure systems and the transport of airflow from the regional areas. The pollution sources include local emissions or transported pollution from other areas (e.g., a sand storm from Mongolian Plateau, as well as primary or secondary pollution from NCP). High-PM episodes also involve complex chemical reactions. In this study, the chemical conversion involves photochemical oxidation and multiphase reactions. While SOA formation was in general mainly affected by the photochemical reactions throughout the campaign, SOA formation facilitated by multiphase reactions was still observed in some periods (e.g., PE1).

In our study, the clean period CP was less affected by regional transport and local accumulation, and the atmospheric condition was conducive to dispersion of air pollutants. The cause of a high-PM event might stem from combined effects that involve the interplays among weather condition, source strength, and chemical conversion. PE1 was a period of local accumulation and secondary conversion under the control of a high-pressure weather system. Emissions and chemistry both affected PE1 significantly. PE2 was a high-PM event caused by regional transport but it was also affected by local emissions at the later stage. Source and meteorology

were the most important factors in the development of PE2. DP was a more complex period, with the atmospheric circulation bringing dust from desert areas to Shanghai. The emissions and chemical processes during DP were changing, along with the meteorological conditions. In the last two stages of DP (DP3 and DP4), the anthropogenic air pollutants (e.g., VOCs) were swept out into the sea and flew back, with oxidation occurring in between contributing to SOA formation. The chemical characteristics (e.g., evolution in terms of O:C vs. H:C ratios) of OA aged over the ocean (DP4) are similar to those over the land (PE2), indicating little dependence of OA characteristics on where the air mass is aged. The results of this study thus suggest that both local primary emissions and secondary formation (both locally and regionally), under the influences of unfavorable meteorological conditions, can induce high-PM episodes. Our results highlight the interactive roles of these three factors in the development of high-PM events, in which one or two of them may be particularly significant. Control measures should be formulated based on the solid understanding of the interplays between these different influencing factors.

CRediT authorship contribution statement

Lulu Zeng: Visualization, Formal analysis, Investigation, Methodology, Writing - original draft. **Dan Dan Huang:** Conceptualization, Supervision, Funding acquisition, Project administration, Investigation, Methodology, Writing - review & editing. **Shuhui Zhu, Fangbing Li, Min Zhou, Liping Qiao, Qian Wang, Qiongqiong Wang, Yingge Ma, Shengrong Lou:** Data Curation, Methodology. **Huabin Shi, Ka In Hoi, Kai Meng Mok, Xinlei Ge:** Methodology, Investigation. **Hongli Wang:** Data Curation, Methodology. **Jian Zhen Yu:** Methodology, Investigation. **Cheng Huang:** Data Curation, Methodology. **Yong Jie Li:** Conceptualization, Supervision, Funding acquisition, Project administration, Investigation, Methodology, Writing - review & editing.

Data availability

Data will be made available on request.

Declaration of competing interest

The authors declare that they have no known competing financial interests or personal relationships that could have appeared to influence the work reported in this paper.

Acknowledgment

This work was supported by the Science and Technology Development Fund, Macau SAR (File no. 023/2021/A1) and Multi-Year Research Grant of University of Macau (No. MYRG2018-00006-FST). Dan Dan Huang acknowledges the financial support from the Shanghai Rising-Star Program (19QB1402900), Shanghai 2021 “Science and Technology Innovation Action Plan” Social Development Science and Technology Project (21DZ1202300), the Science and Technology Commission of the Shanghai Municipality (21230711000).

Appendix A. Supplementary data

Supplementary data to this article can be found online at <https://doi.org/10.1016/j.scitotenv.2022.158347>.

References

- Ait-Helal, W., Borbon, A., Sauvage, S., de Gouw, J.A., Colomb, A., Gros, V., et al., 2014. Volatile and intermediate volatility organic compounds in suburban Paris: variability, origin and importance for SOA formation. *Atmos. Chem. Phys.* 14, 10439–10464.
- Albrecht, B.A., 1989. Aerosols, cloud microphysics, and fractional cloudiness. *Science* 245, 1227–1230.
- An, Z., Huang, R.J., Zhang, R., Tie, X., Li, G., Cao, J., et al., 2019. Severe haze in northern China: a synergy of anthropogenic emissions and atmospheric processes. *Proc. Natl. Acad. Sci. U. S. A.* 116, 8657–8666.
- Brook, R.D., Rajagopalan, S., Pope 3rd, C.A., Brook, J.R., Bhatnagar, A., Diez-Roux, A.V., et al., 2010. Particulate matter air pollution and cardiovascular disease: an update to the scientific statement from the American Heart Association. *Circulation* 121, 2331–2378.
- Cao, L.M., Huang, X.F., Li, Y.Y., Hu, M., He, L.Y., 2018. Volatility measurement of atmospheric submicron aerosols in an urban atmosphere in southern China. *Atmos. Chem. Phys.* 18, 1729–1743.
- Cheng, N., Li, Y., Cheng, B., Wang, X., Meng, F., Wang, Q., et al., 2018. Comparisons of two serious air pollution episodes in winter and summer in Beijing. *J. Environ. Sci. (China)* 69, 141–154.
- Clegg, S.L., Brimblecombe, P., Wexler, A.S., 1998. Thermodynamic model of the system H+ – NH4+ – SO42– – NO3– – H2O at tropospheric temperatures. *J. Phys. Chem. A* 102, 2137–2154.
- Ervens, B., 2004. A modeling study of aqueous production of dicarboxylic acids: 1. Chemical pathways and speciated organic mass production. *J. Geophys. Res.* 109.
- Fiore, A.M., Naik, V., Leibensperger, E.M., 2015. Air quality and climate connections. *J. Air Waste Manag. Assoc.* 65, 648–685.
- Forster, P., Ramaswamy, V., Artaxo, P., Bernntsen, T., Betts, R., Fahey, D.W., et al., 2007. Changes in Atmospheric Constituents and in Radiative Forcing Chapter 2. Cambridge University Press, United Kingdom.
- He, X., Wang, Q.Q., Huang, X.H.H., Huang, D.D., Zhou, M., Qiao, L.P., et al., 2020. Hourly measurements of organic molecular markers in urban Shanghai, China: observation of enhanced formation of secondary organic aerosol during particulate matter episodic periods. *Atmos. Environ.* 240, 117807.
- Heald, C.L., Kroll, J.H., Jimenez, J.L., Docherty, K.S., DeCarlo, P.F., Aiken, A.C., et al., 2010. A simplified description of the evolution of organic aerosol composition in the atmosphere. *Geophys. Res. Lett.* 37.
- Hu, W., Hu, M., Hu, W.W., Zheng, J., Chen, C., Wu, Y.S., et al., 2017. Seasonal variations in high time-resolved chemical compositions, sources, and evolution of atmospheric submicron aerosols in the megacity Beijing. *Atmos. Chem. Phys.* 17, 9979–10000.
- Hu, R., Wang, S., Zheng, H., Zhao, B., Liang, C., Chang, X., et al., 2022. Variations and sources of organic aerosol in winter Beijing under markedly reduced anthropogenic activities during COVID-2019. *Environ. Sci. Technol.* 56, 6956–6967.
- Huang, K., Zhuang, G., Lin, Y., Fu, J.S., Wang, Q., Liu, T., et al., 2012. Typical types and formation mechanisms of haze in an Eastern Asia megacity, Shanghai. *Atmos. Chem. Phys.* 12, 105–124.
- Huang, R.J., Zhang, Y., Bozzetti, C., Ho, K.F., Cao, J.J., Han, Y., et al., 2014. High secondary aerosol contribution to particulate pollution during haze events in China. *Nature* 514, 218–222.
- Huang, R.J., Wang, Y.C., Cao, J.J., Lin, C.S., Duan, J., Chen, Q., et al., 2019. Primary emissions versus secondary formation of fine particulate matter in the most polluted city (Shijiazhuang) in North China. *Atmos. Chem. Phys.* 19, 22823–2299.
- Huang, D.D., Zhu, S., An, J., Wang, Q., Qiao, L., Zhou, M., et al., 2021a. Comparative assessment of cooking emission contributions to urban organic aerosol using online molecular tracers and aerosol mass spectrometry measurements. *Environ. Sci. Technol.* 55, 14526–14535.
- Huang, X., Ding, A., Gao, J., Zheng, B., Zhou, D., Qi, X., et al., 2021b. Enhanced secondary pollution offset reduction of primary emissions during COVID-19 lockdown in China. *Natl. Sci. Rev.* 8, nwaa137.
- Huang, X.F., Cao, L.M., Tian, X.D., Zhu, Q., Saikawa, E., Lin, L.L., et al., 2021c. Critical role of simultaneous reduction of atmospheric odd oxygen for winter haze mitigation. *Environ. Sci. Technol.* 55, 11557–11567.
- Jin, L., Luo, X., Fu, P., Li, X., 2017. Airborne particulate matter pollution in urban China: a chemical mixture perspective from sources to impacts. *Natl. Sci. Rev.* 4, 593–610.
- Kautzman, K.E., Surratt, J.D., Chan, M.N., Chan, A.W., Hersey, S.P., Chhabra, P.S., et al., 2010. Chemical composition of gas- and aerosol-phase products from the photooxidation of naphthalene. *J. Phys. Chem. A* 114, 913–934.
- Lee, B.P., Li, Y.J., Yu, J.Z., Louie, P.K.K., Chan, C.K., 2013. Physical and chemical characterization of ambient aerosol by HR-ToF-AMS at a suburban site in Hong Kong during springtime 2011. *J. Geophys. Res. Atmos.* 118, 8625–8639.
- Lee, B.P., Li, Y.J., Yu, J.Z., Louie, P.K.K., Chan, C.K., 2015. Characteristics of submicron particulate matter at the urban roadside in downtown Hong Kong—overview of 4 months of continuous high-resolution aerosol mass spectrometer measurements. *J. Geophys. Res. Atmos.* 120, 7040–7058.
- Leung, D.M., Shi, H.R., Zhao, B., Wang, J., Ding, E.M., Gu, Y., et al., 2020. Wintertime particulate matter decrease buffered by unfavorable chemical processes despite emissions reductions in China. *Geophys. Res. Lett.* 47, e2020GL087721.
- Li, L.J., Wang, Y., Zhang, Q., Li, J.X., Yang, X.G., Jin, J., 2008. Wheat straw burning and its associated impacts on Beijing air quality. *Sci. China. Ser. D Earth Sci.* 51, 403–414.
- Li, Y.J., Lee, B.P., Su, L., Fung, J.C.H., Chan, C.K., 2015. Seasonal characteristics of fine particulate matter (PM) based on high-resolution time-of-flight aerosol mass spectrometric (HR-ToF-AMS) measurements at the HKUST supersite in Hong Kong. *Atmos. Chem. Phys.* 15, 37–53.
- Li, Y.J., Sun, Y., Zhang, Q., Li, X., Li, M., Zhou, Z., et al., 2017. Real-time chemical characterization of atmospheric particulate matter in China: a review. *Atmos. Environ.* 158, 270–304.
- Li, J.Y., Cao, L.M., Gao, W.K., He, L.Y., Yan, Y.C., He, Y.X., et al., 2021a. Seasonal variations in the highly time-resolved aerosol composition, sources and chemical processes of background submicron particles in the North China plain. *Atmos. Chem. Phys.* 21, 4521–4539.
- Li, J.Y., Gao, W.K., Cao, L.M., He, L.Y., Zhang, X.H., Yan, Y.C., et al., 2021. Effects of different stagnant meteorological conditions on aerosol chemistry and regional transport changes in Beijing, China. *Atmos. Environ.* 258, 118483.
- Liu, P., Song, M., Zhao, T., Gunthe, S.S., Ham, S., He, Y., et al., 2018. Resolving the mechanisms of hygroscopic growth and cloud condensation nuclei activity for organic particulate matter. *Nat. Commun.* 9, 4076.
- Liu, Y., Zheng, M., Yu, M.Y., Cai, X.H., Du, H.Y., Li, J., et al., 2019. High-time-resolution source apportionment of PM2.5 in Beijing with multiple models. *Atmos. Chem. Phys.* 19, 6595–6609.
- Liu, X., Bai, X., Tian, H., Wang, K., Hua, S., Liu, H., et al., 2020. Fine particulate matter pollution in North China: seasonal-spatial variations, source apportionment, sector and regional transport contributions. *Environ. Res.* 184, 109368.
- Lohmann, U., Feichter, J., 2005. Global indirect aerosol effects: a review. *Atmos. Chem. Phys.* 5, 715–737.
- Ma, T., Duan, F., He, K., Qin, Y., Tong, D., Geng, G., et al., 2019. Air pollution characteristics and their relationship with emissions and meteorology in the Yangtze River Delta region during 2014–2016. *J. Environ. Sci. (China)* 83, 8–20.
- Middlebrook, A.M., Bahreini, R., Jimenez, J.L., Canagaratna, M.R., 2012. Evaluation of composition-dependent collection efficiencies for the aerodyne aerosol mass spectrometer using field data. *Aerosol Sci. Technol.* 46, 258–271.
- Ng, N.L., Canagaratna, M.R., Zhang, Q., Jimenez, J.L., Tian, J., Ulbrich, I.M., et al., 2010. Organic aerosol components observed in northern hemispheric datasets from aerosol mass spectrometry. *Atmos. Chem. Phys.* 10, 4625–4641.
- Paatero, P., Hopke, P.K., Song, X.H., Ramadan, Z., 2002. Understanding and controlling rotations in factor analytic models. *Chemom. Intell. Lab. Syst.* 60, 253–264.
- Petters, M.D., Kreidenweis, S.M., 2007. A single parameter representation of hygroscopic growth and cloud condensation nucleus activity. *Atmos. Chem. Phys.* 7, 1961–1971.
- Ramanathan, V., Crutzen, P.J., Kiehl, J.T., Rosenfeld, D., 2001. Aerosols, climate, and the hydrological cycle. *Science* 294, 2119–2124.
- Schauer, J.J., Kleeman, M.J., Cass, G.R., Simoneit, B.R., 2002. Measurement of emissions from air pollution sources. 5. C1–C32 organic compounds from gasoline-powered motor vehicles. *Environ. Sci. Technol.* 36, 1169–1180.
- Seinfeld, J.H., Pandis, S.N., 2016. Atmospheric Chemistry and Physics: From Air Pollution to Climate Change. John Wiley & Sons.
- Stein, A.F., Draxler, R.R., Rolph, G.D., Stunder, B.J.B., Cohen, M.D., Ngan, F., 2015. Noaa's hysplit atmospheric transport and dispersion modeling system. *Bull. Am. Meteorol. Soc.* 96, 2059–2077.
- Sun, Y.L., Jiang, Q., Wang, Z.F., Fu, P.Q., Li, J., Yang, T., et al., 2014. Investigation of the sources and evolution processes of severe haze pollution in Beijing in January 2013. *J. Geophys. Res. Atmos.* 119, 4380–4398.
- Sun, Y., Chen, C., Zhang, Y., Xu, W., Zhou, L., Cheng, X., et al., 2016a. Rapid formation and evolution of an extreme haze episode in northern China during winter 2015. *Sci. Rep.* 6, 27151.
- Sun, Y.L., Du, W., Fu, P.Q., Wang, Q.Q., Li, J., Ge, X.L., et al., 2016b. Primary and secondary aerosols in Beijing in winter: sources, variations and processes. *Atmos. Chem. Phys.* 16, 8309–8329.
- Tian, Y., Pan, X.L., Nishizawa, T., Kobayashi, H., Uno, I., Wang, X.Q., et al., 2018. Variability of depolarization of aerosol particles in the megacity of Beijing: implications for the interaction between anthropogenic pollutants and mineral dust particles. *Atmos. Chem. Phys.* 18, 18203–18217.
- Tong, S.Y., Kong, L.D., Yang, K.J., Shen, J.D., Chen, L., Jin, S.Y., et al., 2020. 238. *Atmos. Environ.* 117756.
- Twomey, S., 1977. The influence of pollution on the shortwave albedo of clouds. *J. Atmos. Sci.* 34, 1149–1152.
- Ulbrich, I.M., Canagaratna, M.R., Zhang, Q., Worsnop, D.R., Jimenez, J.L., 2009. Interpretation of organic components from positive matrix factorization of aerosol mass spectrometric data. *Atmos. Chem. Phys.* 9, 2891–2918.
- Wang, H., Lyu, X.P., Guo, H., Wang, Y., Zou, S.C., Ling, Z.H., et al., 2018a. Ozone pollution around a coastal region of South China Sea: interaction between marine and continental air. *Atmos. Chem. Phys.* 18, 4277–4295.

- Wang, Y., Guo, H., Zou, S., Lyu, X., Ling, Z., Cheng, H., et al., 2018b. Surface O₃ photochemistry over the South China Sea: application of a near-explicit chemical mechanism box model. *Environ. Pollut.* 234, 155–166.
- Wang, M., Huang, R.J., Cao, J.J., Dai, W.T., Zhou, J.M., Lin, C.S., et al., 2019a. Determination of n-alkanes, polycyclic aromatic hydrocarbons and hopanes in atmospheric aerosol: evaluation and comparison of thermal desorption GC-MS and solvent extraction GC-MS approaches. *Atmos. Meas. Techn.* 12, 4779–4789.
- Wang, Y., Chen, J., Wang, Q., Qin, Q., Ye, J., Han, Y., et al., 2019b. Increased secondary aerosol contribution and possible processing on polluted winter days in China. *Environ. Int.* 127, 78–84.
- Wang, X., Wang, C.Z., Wu, J., Miao, G.F., Chen, M., Chen, S.L., et al., 2021. Intermediate aerosol loading enhances photosynthetic activity of croplands. *Geophys. Res. Lett.* 48, e2020GL091893.
- Watson, J.G., 2002. Visibility: science and regulation. *J. Air Waste Manag. Assoc.* 52, 628–713.
- Wood, E.C., Canagaratna, M.R., Herndon, S.C., Onasch, T.B., Kolb, C.E., Worsnop, D.R., et al., 2010. Investigation of the correlation between odd oxygen and secondary organic aerosols in Mexico City and Houston. *Atmos. Chem. Phys.* 10, 8947–8968.
- Wu, M., Wu, D., Fan, Q., Wang, B.M., Li, H.W., Fan, S.J., 2013. Observational studies of the meteorological characteristics associated with poor air quality over the Pearl River Delta in China. *Atmos. Chem. Phys.* 13, 10755–10766.
- Wu, C., Zhang, S., Wang, G., Lv, S., Li, D., Liu, L., et al., 2020. Efficient heterogeneous formation of ammonium nitrate on the saline mineral particle surface in the atmosphere of East Asia during dust storm periods. *Environ. Sci. Technol.* 54, 15622–15630.
- Xing, Y.F., Xu, Y.H., Shi, M.H., Lian, Y.X., 2016. The impact of PM2.5 on the human respiratory system. *J. Thorac. Dis.* 8, E69–E74.
- Xu, W.Y., Zhao, C.S., Ran, L., Deng, Z.Z., Liu, P.F., Ma, N., et al., 2011. Characteristics of pollutants and their correlation to meteorological conditions at a suburban site in the North China plain. *Atmos. Chem. Phys.* 11, 4353–4369.
- Xu, J.M., Yan, F.X., Xie, Y., Wang, F.Y., Wu, J.B., Fu, Q.Y., 2015. Impact of meteorological conditions on a nine-day particulate matter pollution event observed in December 2013, Shanghai, China. *Particuology* 20, 69–79.
- Xu, W., Han, T., Du, W., Wang, Q., Chen, C., Zhao, J., et al., 2017. Effects of Aqueous-Phase and Photochemical Processing on Secondary Organic Aerosol Formation and Evolution in Beijing, China. *Environ. Sci. Technol.* 51, 762–770.
- Yang, Y.R., Liu, X.G., Qu, Y., An, J.L., Jiang, R., Zhang, Y.H., et al., 2015. Characteristics and formation mechanism of continuous hazes in China: a case study during the autumn of 2014 in the North China plain. *Atmos. Chem. Phys.* 15, 8165–8178.
- Yang, S., Duan, F., Ma, Y., Li, H., Ma, T., Zhu, L., et al., 2020. Mixed and intensive haze pollution during the transition period between autumn and winter in Beijing, China. *Sci. Total Environ.* 711, 134745.
- Yue, X., Unger, N., Harper, K., Xia, X.G., Liao, H., Zhu, T., et al., 2017. Ozone and haze pollution weakens net primary productivity in China. *Atmos. Chem. Phys.* 17, 6073–6089.
- Zhang, Q., Jimenez, J.L., Canagaratna, M.R., Ulbrich, I.M., Ng, N.L., Worsnop, D.R., et al., 2011. Understanding atmospheric organic aerosols via factor analysis of aerosol mass spectrometry: a review. *Anal. Bioanal. Chem.* 401, 3045–3067.
- Zhang, Y.J., Tang, L.L., Wang, Z., Yu, H.X., Sun, Y.L., Liu, D., et al., 2015. Insights into characteristics, sources, and evolution of submicron aerosols during harvest seasons in the Yangtze River delta region, China. *Atmos. Chem. Phys.* 15, 1331–1349.
- Zhang, L.B., Liu, Y.Q., Hao, L., 2016. Contributions of open crop straw burning emissions to PM_{2.5} concentrations in China. *Environ. Res. Lett.* 11, 014014.
- Zhang, Y., Wang, Y., Zhang, X., Shen, X., Sun, J., Wu, L., et al., 2018. Chemical components, variation, and source identification of PM₁ during the heavy air pollution episodes in Beijing in December 2016. *J. Meteorol. Res.* 32, 1–13.
- Zhong, J.T., Zhang, X.Y., Dong, Y.S., Wang, Y.Q., Liu, C., Wang, J.Z., et al., 2018. Feedback effects of boundary-layer meteorological factors on cumulative explosive growth of PM_{2.5} during winter heavy pollution episodes in Beijing from 2013 to 2016. *Atmospheric Chemistry and Physics* 18, 247–258.
- Zhu, S., Wang, Q., Qiao, L., Zhou, M., Wang, S., Lou, S., et al., 2021a. Tracer-based characterization of source variations of PM_{2.5} and organic carbon in Shanghai influenced by the COVID-19 lockdown. *Faraday Discuss.* 226, 112–137.
- Zhu, S., Wang, Q., Qiao, L., Zhou, M., Wang, S., Lou, S., et al., 2021b. Tracer-based characterization of source variations of PM_{2.5} and organic carbon in Shanghai influenced by the COVID-19 lockdown. *Faraday Discuss.* 226, 112–137.
- Zhu, W., Zhou, M., Cheng, Z., Yan, N., Huang, C., Qiao, L., et al., 2021c. Seasonal variation of aerosol compositions in Shanghai, China: insights from particle aerosol mass spectrometer observations. *Sci. Total Environ.* 771, 144948.